Scientia Iranica B (2023) 30(2), 391–408

Sharif University of Technology
Scientia Iranica
Transactions B: Mechanical Engineering
http://scientiairanica.sharif.edu

Artificial neural network-based predictive model for output characteristics in drilling of quartz cyanate ester polymeric composite

T. Ramalingam[a,*], N. Kishore Nath[a], and N. Selvaraj[b]

a. *Advanced Systems Laboratory, DRDO, Hyderabad, Telangana, India, 500058.*
b. *Department of Mechanical Engineering, National Institute of Technology, Warangal, Telangana, India, 506004.*

Received 26 October 2021; received in revised form 19 July 2022; accepted 1 October 2022

KEYWORDS
ANN;
BPNN;
Quartz polymeric composite;
Drilling;
Resin transfer molding.

Abstract. Apart from the widely used polymeric fibers, Quartz fiber is the one that possesses various characteristics. Quartz polymeric fiber in combination with Cyanate Ester resin produces a high-performance composite that has excellent properties and is used primarily in military applications. The present investigation aims at developing a model to predict the output characteristics of hole in the drilling of Quartz composite laminate. Output parameters considered are thrust force, torque, exit delamination factor, hole diameter, cylindricity, and surface roughness. Vacuum Assisted Resin Transfer Molding (VARTM) process was adopted for laminate manufacturing. Full factorial design of experiments was considered for the selected input parameters and experiments were carried out. Further modeling was developed to predict the output parameters employing Back Propagation Neural Network (BPNN) method and it was found that the optimal network architecture was 3-45-15-10-6 with Mean Squared Error (MSE) of 0.0105. Experimental results were analyzed and the influence of input parameters in this drilling process was studied. The testing data were consistent with the output parameters predicted from the model and the obtained maximum error was 7.58%. Further, the model developed was validated with a new batch of experiments and the values obtained were satisfactory with maximum error of 7.17%.

1. Introduction

Composite is a combination of one or more than one constituent. It possesses various advantages in terms of stiffness, strength, and various other properties. Each application demands a specific property. In recent years, composite has been widely used in various applications. Composites are classified broadly on the basis of raw material used in reinforcement and matrix. Based on the reinforcement, widely used composites are Glass Fiber Reinforced Plastics (GFRP), Carbon Fiber Reinforced Plastics (CFRP), and Aramid Fiber Reinforced Plastics (AFRP). These composites are used in commercial, aerospace, and military applications and their uses are widespread. Apart from these, there are other fibers that can be used in composite structures. One among them is quartz fiber. Quartz polymeric

*. *Corresponding author. Tel.: +91-9490747246*
E-mail addresses: t.ramling@gmail.com (T. Ramalingam); lca_droptank@yahoo.com (N. Kishore Nath); selva@nitw.ac.in (N. Selvaraj)

doi: 10.24200/sci.2022.59238.6129

fiber is made from high-purity quartz crystal where SiO_2 content is more than 99.95%. Quartz possesses various characteristics such as strength retainment at high temperatures, low thermal expansion, good thermal shock resistance, better chemical stability, electromagnetic transparency, electric insulation, and high temperature applications safely up to 1100°C.

Quartz polymer has an excellent combination of structural and electromagnetic properties that can be used as high-performance composite materials. It is mainly suited for components where low electromagnetic interference characteristics are the prime requirements along with good strength-to-weight ratios. This material is primarily used for radome of fighter aircraft in military applications [1] because of low electromagnetic characteristics compared to other available polymeric fibers. In the fabrication of composite components, basically two processes are involved: primary operation and secondary operation. Primary operations are generally automated processes like filament winding, Resin Transfer Molding (RTM), and compression molding and the components using any of these processes are considered in the shape close to the final one; however, these components need to be joined to other sub-systems and are generally done by means of fasteners and rivets. To the same end, component requires hole done by means of secondary operation, namely drilling. It is observed that secondary operations like drilling have not been reported on quartz polymeric composite. Furthermore composites being anisotropic and heterogenous machining is a challenging process compared to machining of conventional metals.

Drilling process in composite can be assessed based on these quality characteristics such as delamination factor, hole size, cylindricity, and surface roughness of the hole [2,3]. Among these, delamination is deemed either major or severe form of damage in the drilling of laminated composites. Other important factors that should be considered in determining the quality of hole are the hole size and roundness of a hole along the length. In particular, the need for drilling within specified tolerance threshold with suitable roundness along the length is an element deemed important in the aerospace industry [2]. Hole quality is severely impacted by delamination which causes a considerable reduction in loading capacity and the performances intended [2]. Delamination also reduces the fatigue properties of the structure resulting in the reduction of serviceable life of the composite structure [4,5]. Delamination happens at the entry and exit side in the drilling process of composites. Among the two types of delamination, the one that occurs at the drill exit, also known as push down delamination, is more significant in drilling of composites [6]. Researchers [7,8] performed experiments on different fiber composites and reported that thrust force and torque were the prime reasons for getting poor surface finish and machining induced defects. It was reported that minimization of thrust force resulted in the reduction of these induced defects due to the drilling process [9,10].

Many researchers have studied the effect of various input parameters in the drilling process on the output quality characteristics in CFRP and GFRP composites. There are researchers who have worked on modeling of drilling of widely used glass and carbon polymeric composites. Vijayan et al. [11] investigated CFRP laminates with carbide twist drill varying the drilling parameters and analyzed the hole quality characteristics. Further optimization of machining parameters was done and tool life was predicted. This work revealed that feed rate during drilling had a major impact on thrust force, exit delamination, and measured hole diameter. Anarghya et al. [12] performed studies to reduce the delamination on drilling of AFRP with solid carbide minimizing thrust force and torque. Furthermore, the prediction model using Multilayer Perception Neural Network optimized by Genetic Algorithm (MLPNN-GA) and Response Surface Method (RSM) was developed and compared. This study demonstrated that the principal factor that affects the thrust force was drill point angle and argued that low feed and drill bit with low point angle facilitated reducing delamination. Lee et al. [13] studied the drilling characteristics of CFRP and hybrid C-AFRP for delamination and tool wear with low-point angle carbide drill and suggested that thrust force shall be minimized with low feed rate and proper tool geometry. Kalita et al. [14] performed an extensive experimental investigation into GFRP and developed an empirical model for delamination factor. Genetic Algorithm (GA) and Particle Swarm Optimization (PSO) techniques were employed to derive the optimum input parameters for minimum delamination. Further, this work concluded that feed rate was an important factor and delamination increased with the increase in feed rate. Ali et al. [15] performed research on drilling of pure GFRP composites and added GFRP composites to study the effect of input parameters on delamination using Taguchi method. RSM modeling was done for delamination. Further, the work concluded that the effect of feed rate on damage during drilling was more significant than the cutting speed effect and optimum input parameters were obtained for material removal rate and delamination. Ahmet et al. [16] investigated delamination in CFRP composites due to drilling and concluded that the best outcomes for thrust force and delamination were attained with low feed rate and drill bit with low point angle. Ramesh et al. [17] developed response surface models for different quality characteristics with respect to input parameters employing different drill geometries and studied the effect of the

Table 1. Summary of literature and analyzed parameters in drilling polymeric composites.

Ref.	Workpiece material	Analysed parameters
[11]	CFRP	Hole diameter, circularity, delamination
[12]	AFRP	Thrust force, Torque
[13]	CFRP & C-AFRP	Thrust force, Tool wear
[14]	GFRP	Delamination
[15]	GFRP	Delamination
[16]	CFRP	Thrust force, delamination
[17]	CFRP	Thrust force, torque, surface roughness, ovality, delamination

process parameters. Table 1 shows the synopsis of the explained literature in drilling of polymeric composites and measured output responses.

Although numerous studies have investigated drilling of composites, particularly in CFRP and GFRP, none to date has investigated the effect of cutting parameters on the drilling of quartz polymeric composites. Further to this, the neural network modeling for the output characteristics has not been applied in drilling of quartz composite material. ANN provides effective process modeling in terms of efficiency, accuracy, and cost. The main important feature of neural network modeling is its capability to build a model where data generation is a difficult, expensive and time-taking process [18]. Furthermore, it is reported that the models developed using ANN to predict the parameters show substantial improvement in experimental error [19].

The application of ANN was reported by several researchers who have generated a model for different polymeric composite materials. Karnik et al. [18] developed an ANN model in high-speed drilling of the CFRP composite for the damages induced at the entry of the hole considering the drilling process parameters. Yang et al. [20] developed a neural model using back propagation learning algorithm to predict the residual strength under compression after impact loading of CFRP composites. In this work, finite element model results after validation were used to establish a nonlinear relationship with the input parameters. Guoqiang et al. [21] developed a neural network model for predication of different states of tool wear during machining of composite materials. Qian and Xiaoliang [22] developed a neural network model for expressing output characteristics as a function of drilling input parameters in CFRP composite. Further multiple objective optimization of input parameters was done with thrust force, delamination factor, and material removal rate as objectives. Soepangkat et al. [23] applied an integrated approach to the prediction of multi-performance characteristics and further optimized the drilling process of AFRP composite. Fajar et al. [24] investigated the effect of the process parameters on surface roughness and delamination in the end-milling process of CFRP composite and further developed a network model using back propagation method for the outputs. Vineela et al. [25] predicted the ultimate tensile strength of hybrid short-fiber composites made of glass and carbon using artificial neural network method. Moreover, the model predicted by ANN was compared with regression analysis and further analyzed. Mishra et al. [26] established an ANN predictive model for estimating the residual tensile strength with a hole in Unidirectional Glass Fiber-Reinforced Plastic (UD-GFRP) composite laminates for the input process parameters. Soepangkat et al. [27] adopted an integrated approach using back propagation neural method and Particle Swarm Optimization (PSO) for modeling and optimizing multiple characteristics of drilling a hole in the CFRP composite laminates. Table 2 shows the synopsis of the explained literature on the neural network modeling of polymeric composites.

Various studies have modeled drilling of various composite materials, particularly in CFRP and GFRP composites. Nevertheless, there is no investigation on quartz polymeric composite drilling to demonstrate a predictive correlation between the output characteristics and input variables. The present work aims to establish a relation among the drilling process input variables, namely spindle speed, feed, and point angle on six output parameters, namely thrust force, torque, delamination factor at exit, hole diameter, cylindricity, and surface roughness using Artificial Neural Network (ANN) method on a quartz polymeric composite.

2. Materials and methods

The Quartz composite sample used in this study was 4 mm thick. Quartz reinforcement is available in yarn form. Source of quartz yarn is from M/s Saint Gobain, France and the matrix material cyanate ester resin is from M/s Toray Advanced Composites, USA. Yarn

Table 2. Summary of literature in neural network modeling of polymeric composites.

Ref.	Workpiece material	Model developed for parameters
[18]	CFRP	Delamination
[20]	CFRP	Residual strength
[21]	CFRP	Tool wear
[22]	CFRP	Thrust force and delamination
[23]	AFRP	Thrust force, torque, delamination, surface roughness, roundness
[24]	CFRP	Delamination, surface roughness
[25]	CFRP & GFRP	Tensile strength
[26]	GFRP	Residual tensile strength
[27]	CFRP	Thrust force, torque, delamination

Figure 1. Woven fabric with quartz yarn.

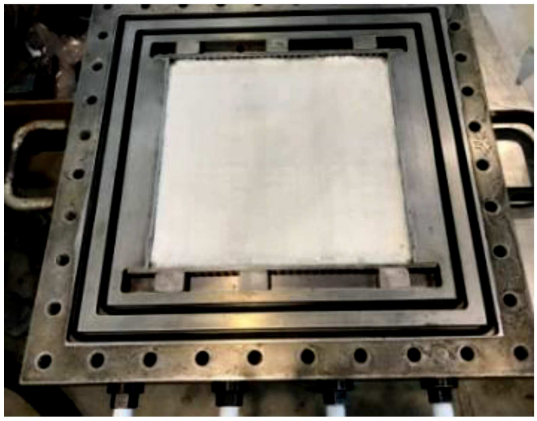

Figure 2. Quartz fabric in mold.

is woven into fabric of 2 × 2 twill weave with 300 GSM, as shown in Figure 1. Quartz composite laminate was fabricated by Vacuum Assisted Resin Transfer Moulding (VARTM) method.

In the VARTM process, mold with bottom and top portions is taken and woven quartz fabric of predetermined size is placed on the cavity. The cavity of the mold determines the thickness of the composite. Thirteen layers of reinforcement are cut into 300 mm × 300 mm and placed in the mold cavity, as shown in Figure 2. Preheated cyanate ester resin at 40°C with viscosity of 100-150 cP suitable for this process is injected under vacuum of 700 mm of Hg. After resin injection, the laminate is cured at 180°C. The thickness of the laminate after curing is 4 mm. Fiber volume fraction (V_f) for the cured laminate is measured at 55%. Also, degree of cure by Digital Scanning Calorimetry (DSC) and through transmission Non-Destructive Evaluation (NDE) was done to ascertain the quality of laminate. Workpiece Specimen of 100 mm × 100 mm is cut from the realized laminate for the drilling experiments.

Drilling tests were examined through BFW Gaurav BMV 35 TC 20 Vertical Machining Center (VMC) CNC machine. A schematic diagram of the experimental setup is shown in Figure 3. Specimen was assembled to machine table with the use of fixture. Feed (f), drill bit point angle (θ), and speed (N) are input parameters and their respective levels are tabulated in Table 3.

A Full Factorial Design (FFD) of experiment was performed with the input parameters. A total of 27 tests were conducted and each test was performed thrice. The average of the result is considered and reported. Spindle speed, point angle, and feed are considered as machine inputs. Tungsten Carbide (TC) "k20 grade twist drill bit" was utilized for carrying out experiments. Drills have a diameter of 5 mm and helix angle of 30°. Range of each parameter was finalized after performing trial experiments. All the experiments were performed without the use of coolant.

Table 3. Input parameters.

Parameters	Level 1	Level 2	Level 3
Spindle speed, N (rpm)	500	1000	1500
Feed, f (mm.rev^{-1})	0.05	0.10	0.15
Point angle, θ (°)	85	118	135

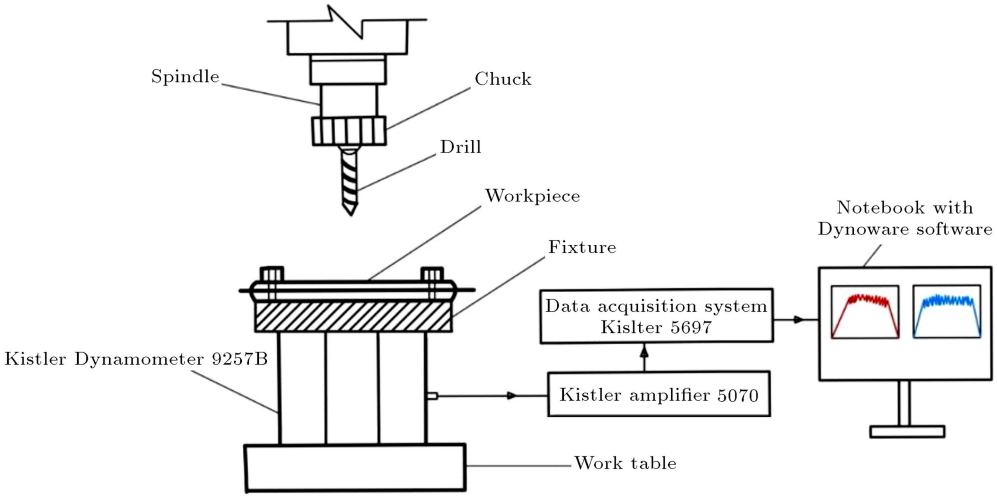

Figure 3. Schematic diagram of the experimental setup.

2.1. Measurement plan

2.1.1. Thrust force and torque

"Kistler 9257B Piezoelectric Dynamometer" was utilized for measuring torque (T) and thrust force (F_z) during the experiments. Dynamometer output is connected to a Kistler charge amplifier 5070, thereby signal is amplified commensurate to the load applied and further, the signal is digitized with A/D convertor. Digitized signal is transmitted to a notebook installed with DynoWare software to store the torque and thrust force graphs. Torque and thrust forces were continuously observed, as shown in Figure 4, and the test results were noted.

Figure 4. Experimental test setup on machine.

2.1.2. Exit delamination factor

The damages were evaluated in quantitative terms after the drill test. Two mechanisms of delamination occur in composites. One is peel-up delamination at entry of the hole and the other one is delamination at the exit of the drilled hole. Effect of damage induced at the exit is more severe than the one at entry [6]. In this study, delamination factor at exit is considered. Delamination factor was estimated using the image of lower surface of each specimen scanned by an optical microscope. The image scanned using "OGP Flash 200" is stored as a bitmap image and, then, imported to image processing software namely "Image-J" to analyze the image. Delamination factor (F_d) is estimated using Eq. (1):

$$F_d = \frac{D_{\max}}{D_o}, \tag{1}$$

where $D_{\max}$ is the maximum diameter of the hole drilled with delaminated zone and D_0 is the nominal diameter of the drill [28]. Figure 5 explains the scheme for measuring the delamination factor.

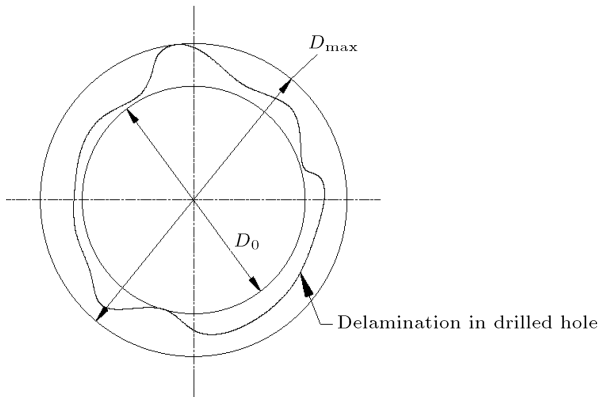

Figure 5. Scheme for measurement of delamination factor.

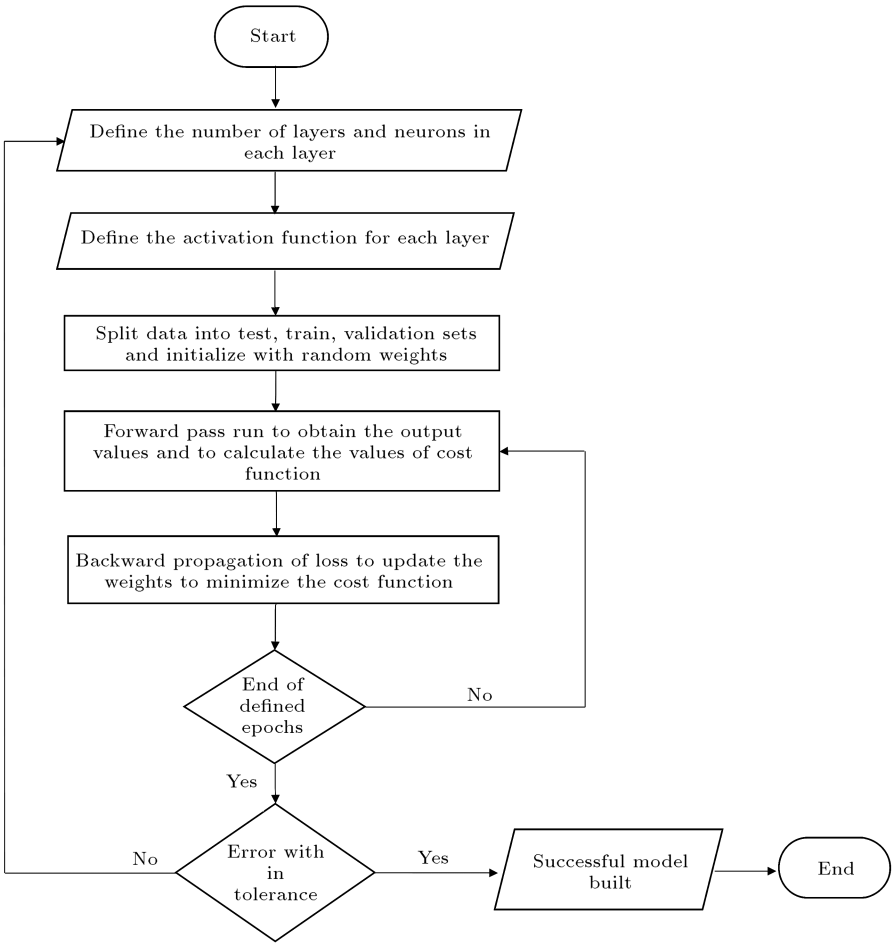

Figure 6. Steps involved in the development of artificial neural network model.

2.1.3. Hole diameter and cylindricity

Hole diameters (D) and cylindricity (ϕ) were analyzed using "DEA Global advantage Co-ordinate Measuring Machine (CMM)" with a ruby probe of 1 mm diameter.

2.1.4. Surface roughness

Surface roughness (R_a) was estimated using "Zeiss Surfcom-1900SD" surface measuring device along the hole wall surface parallel to the drill direction at six different locations, and the average of six measurements along the hole wall was considered.

2.2. Back Propagation Neural Network (BPNN) model

ANN plays a vital role in predicting the solution to problems in various engineering fields. Various learning strategies are applied in the ANN to produce a desired output. One such strategy for learning is Back Propagation Neural Network (BPNN) method.

This method is chosen due to the reason that this scheme has multiple merits over the other available networks, and other applications have used successfully this method [29,30]. In BPNN neural networks, there are two steps involved with respect to training the neural network. The first one is forward feed and the next one is back propagation. Figure 6 explains the step involved in the development of ANN model.

3. ANN training

Figure 7 describes the multi-layer ANN architecture developed for the current problem. The architecture has an input layer that comprises three neurons for feed, cutting speed, point angle of cutting tool and six neurons in the output layer for drilling output characteristics namely Thrust force (F_z), torque (T), delamination factor at exit (F_d), hole diameter (D), cylindricity (ϕ), and surface roughness (R_a).

In the architecture model, the activation value (Z_j) to the jth neuron is given as [27].

$$Z_j = \left(\sum_{i=1}^{i=i} (u_{ij} * x_i) \right) + u_{oj}, \tag{2}$$

where i is the number of input neurons in the input layer, j the number of neurons in the first hidden layer, u_{oj} the bias for the first hidden layer, u_{ij} the weight

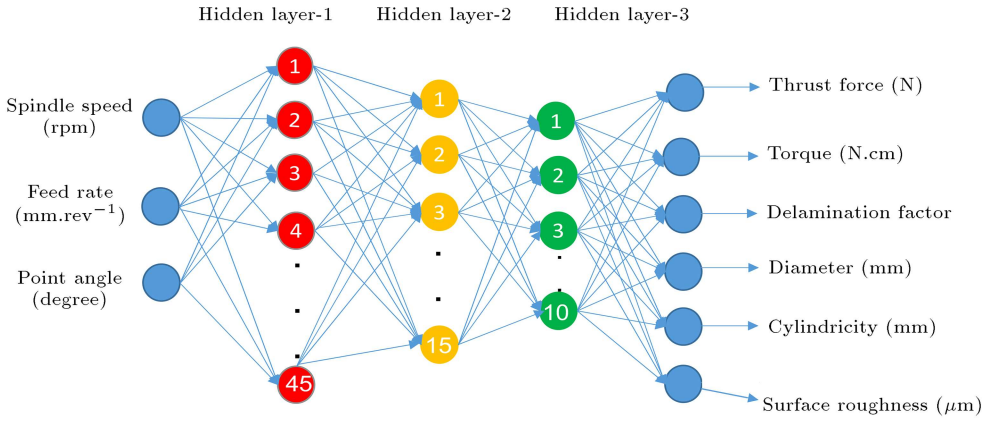

Figure 7. Developed artificial neural network architecture for the present investigation.

on the ith input neuron to the jth neuron on the first hidden layer and x_i the ith input neuron value.

For a hyperbolic tangent activation function, the objective function (O_j) for the jth neuron in the hidden layer 1 is given as:

$$O_j = \tanh(Z_j). \tag{3}$$

Similarly, the activation value and objective function for hidden layers 2 and 3 are derived by considering the outputs of the preceding layer as input and using the bias value of the respective layer with hyperbolic tangent activation function.

BPNN employs a gradient search method and it is based on the updating of weights to reduce the sum of mean squared error to a minimum. The optimizer uses squared gradients moving average for each weight. The weights of the links [31] are updated as follows:

$$E\left[g^2\right]_t = \beta E\left[g^2\right]_{t-1} + (1-\beta)\, g_t^2, \tag{4}$$

$$u_t = u_{t-1} - \left(\frac{\eta}{\left(\sqrt{E\left[g^2\right]_t}\right)} * g_t\right), \tag{5}$$

where $E\left[g^2\right]_t$ is the squared gradients moving average, g_t the gradient of the cost function with respect to the weight u, η the learning rate, β the moving average parameter, u_t the updated weights of a particular neuron in a layer and u_{t-1} the weights of a particular neuron in a layer before updating.

Error (E) for one set of input values is calculated [18] as follows:

$$E = \frac{1}{2}\sum_{K=1}^{K}\left(D_{kp} - O_{kp}\right)^2, \tag{6}$$

where k is the number of neurons in the output layer, D_{kp} the experimental target value of the pth pattern, and O_{kp} the predicted output value of the neural network.

Mean Squared Error (MSE) for one epoch is calculated [18] as follows:

$$MSE = \frac{1}{N_p}\sum_{p=1}^{N_p}\sum_{k=1}^{k}\left(D_{kp} - O_{kp}\right)^2, \tag{7}$$

where N_p is the number of training patterns in one epoch and in the present case, N_p is 21.

The activation value, objective function, weights updating, error, and mean squared error are calculated using Eqs. (2)–(7). BPNN training process starts with assigning small weights randomly to the neurons of the links. The entire training data are then passed through the model and the assigned weight gets updated after the end of each epoch. This process is continued till the summation of the squared error value for output neurons is achieved minimum. Similarly, the neural network training process starts with bias, randomly assigned for each of the hidden layers.

BPNN learning process is iterative. The full data set is repeatedly passed through the neural network until the MSE value reaches an acceptable value. The dataset is split into training and test data. Test data is 10% of the total set including 3 numbers of input-output pattern and the remaining data is for training and validation, i.e., 90% of the data is for training and validation including 24 numbers of input-output pattern. Experimental and predicted outputs for all the responses are given in Appendix A, Tables A.1 and A.2. Further, the training and validation were carried out using first 24 datasets from these two tables (S.No: 1-24), and the remaining 3 data sets (S.No. 25-27) were utilized to test the trained model. Normalization of data was done using standard scalar function.

Then, BPNN training with the normalized datasets was carried out. Jupyter notebook was the Interactive Development Environment (IDE) used for developing the neural network in Python. Deep learning libraries like Keras & Tensor Flow were employed to build and compile the model. The number of hidden layers and neurons in those layers is paramount and

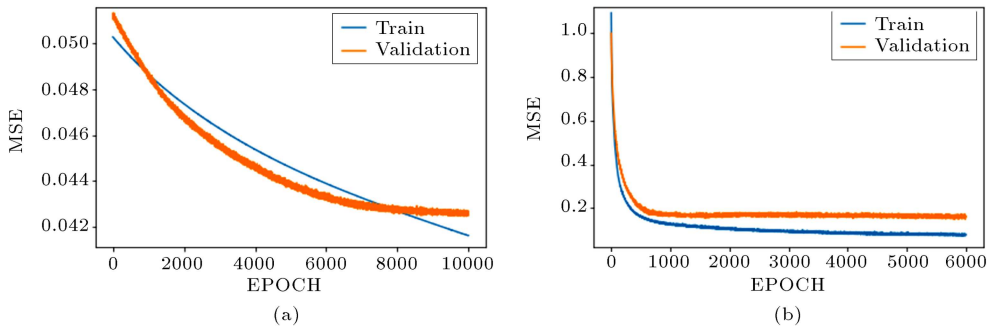

Figure 8. (a) Mean squared error variation for the initial model with one hidden layer. (b) Mean squared error variation for the initial model with three hidden layers.

their selection is critical for a successful training. Input and output data size also influences this selection. In the present study, the criteria for the number of hidden layers and neurons in those layers to determine the architecture considered were 03 and 100, respectively. Activation functions such as hyperbolic tangent, sigmoid, log-sigmoid, ReLu, and LeakyReLu were considered and employed for developing the network during the iterative process. In the current network training, the goal was set to achieve MSE of 0.00001.

RMSprop was the optimizer employed to minimize the cost function, i.e., MSE. Lasso (L1 regularization) and Ridge (L2 regularization) regression were used to limit the overfitting phenomenon and the value for both was fixed to 0.01 in the present model. Learning rates in training are to be defined and the high value makes the convergence process faster, but may lead to non-convergence. More certain and reliable results can be achieved using slow value of learning rates [26]. Thus, in the present network model, the learning rate was kept at 0.1 initially to train the network faster in the high error scenario and it was decreased gradually to 1.5e-4 depending on the reduction of the error value.

Different models were built by the varying number of layers and neurons using considered activation functions. Figure 8(a) and (b) depict the initially developed typical models where the MSE variation is higher with one, three hidden layers and MSE values of the validation data for those models are 0.0431 and 0.192 after epochs of 10000 and 6000, respectively. The corresponding learning parameters for the models are given in Table 4. Each model was trained by tuning hyper parameters to reduce the prediction error. After tuning the parameters with 45, 15, and 10 neurons in first, second, and third hidden layers, satisfactory training was achieved and the same architecture was chosen. MSE variation for the developed architecture is shown in Figure 9. Table 5 shows the learning parameters used for the developed model in this investigation. At the end of the model training, the optimum MSE was 0.0105 after the epoch of 5000.

Table 4. Summary of learning parameters for the initial models with different hidden layers.

Parameters	A	B
Network architecture	3-5-6	3-40-20-10-6
Number of hidden layers	1	3
Activation function used	Tanh	Tanh
Pattern count for training	21	21
Pattern count for testing	3	3
Pattern count for validation	3	3
Sum of mean squared error	0.0277	0.0786
Epoch number	10000	6000
Learning factor	1.5e-4	1e-3
L1 regularisation	0.01	0.01
L2 regularisation	0.01	0.01

Table 5. Summary of learning parameters for the developed model.

Parameters	Values
Number of hidden layers	3
Activation function used	Tanh
Pattern count for training	21
Pattern count for testing	3
Pattern count for validation	3
Sum of mean squared error	0.0105
Epoch number	5000
Learning factor	1.5e-4
L1 regularisation	0.01
L2 regularisation	0.01

4. Results and discussion

4.1. ANN testing

21 datasets used for training were initially employed and the trained network architecture was examined. The predicted values for output parameters were com-

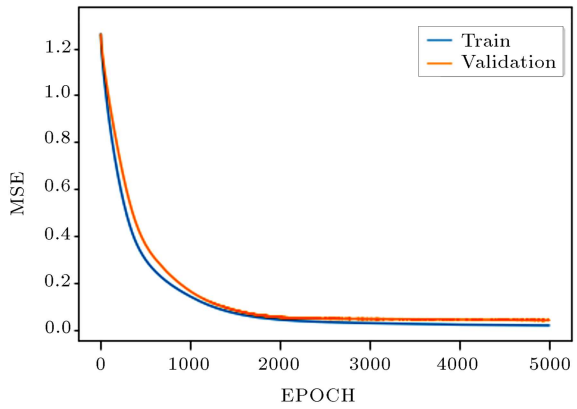

Figure 9. Mean squared error variation for the developed neural network architecture.

pared with the corresponding experimental results for each respective input dataset and the error percentage was determined as per Eq. (8), which is given as:

$$Error\% = \left(\frac{output_{\exp} - output_{pred}}{output_{\exp}}\right) * 100, \qquad (8)$$

where $output_{\exp}$ is the experimental value of all the six output characteristics, and $output_{pred}$ is the predicted value of all the six output characteristics by the network model.

The model found that values of all the six reported output parameters showed a close match to the corresponding experimentally measured values. The bar charts of the experimental and predicted values for all the six output parameters of the training data are given in Appendix B, Figure B.1. It can be noticed that the absolute error was found to be less than 10% for all the cases of six output parameters. Further, the model was examined employing the concluding 3 datasets. The comparison of all the six output parameters for the testing data set between prediction and experimental data is given in Figure B.2. in the form of a bar graph and the error percentage is tabulated in Table 6. It is noticed that the predicted values show a good match with the experimentally determined values and the maximum error among all the output characteristics for testing patterns is found to be 7.58%.

The coefficient of correlation (R-value), denoted by All corr, between the predicted values and experimental outputs was evaluated. If R value is close to 1, then it indicates a better correlation between predicted and actual values [18]. In the current investigation, the overall R value for the entire training, validation, testing data is between 0.9871 and 0.9958, which indicates a good correlation. The overall performance plot of the present model with R-value for the entire dataset denoted by "All corr" is given in Figure 10.

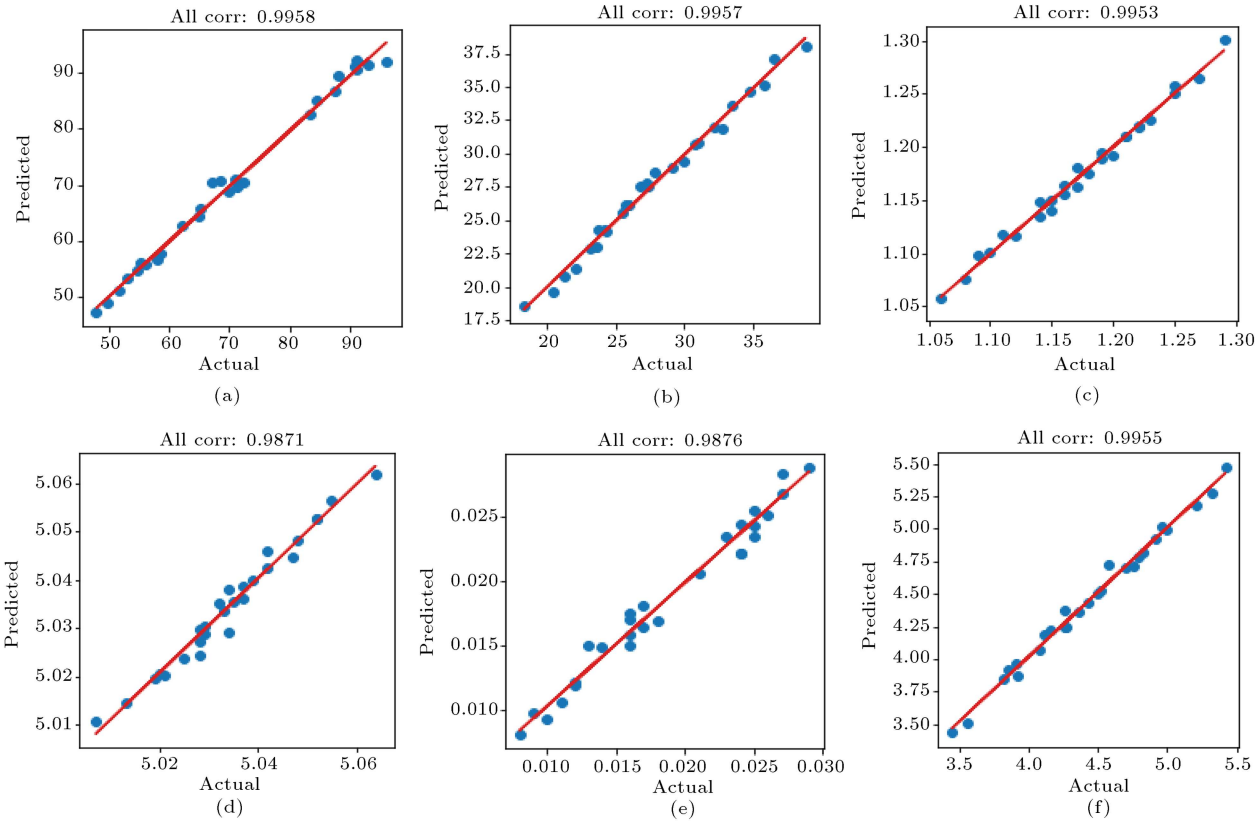

Figure 10. Overall performance of the developed model for (a) Thrust force, (b) torque, (c) delamination factor, (d) diameter, (e) cylindricity, and (f) surface roughness.

Table 6. Error percentage of testing data compared to experimental values.

S. no	Spindle speed (rpm)	Feed rate ($mm.rev^{-1}$)	Point angle (°)	Error percentage of testing data (%)					
				Thrust force (F_z)	Torque (T)	Delamination factor (F_d)	Diameter (D)	Cylindricity (ϕ)	Surface roughness (R_a)
1	500	0.05	85	0.53	2.42	0.68	−0.01	6.39	0.31
2	1000	0.05	85	1.23	3.55	0.72	−0.08	7.58	−1.51
3	1500	0.10	135	−5.03	0.33	−0.43	−0.08	2.76	−1.13

4.2. Model verification

Further, the developed model was validated with the fresh set of experimental values where the four absolutely different new sets of experimental data are considered. This kind of validation process is used to check the viability of the developed neural network model for the new data [30]. The related outputs and error percentage are given in Table 7. It is noticed from the table that the predicted output of the trained model almost follows the experimentally obtained output and the maximum error percentage is 7.17%, which is below the acceptable limit [30].

4.3. Effect of input parameters

Effort was put in the current investigation to evaluate the output characteristics of quartz composite laminate with drilled holes. Scatter plots for experimental values of all the output parameters are presented and discussed in this section. Figure 11 shows the processed image of exit location of drilled holes at constant speed and feed for different point angles. Regarding the point angle effect on torque and thrust force, increase in point angle raises the effect of chisel edge of drill bit, thus producing more torque and thrust force. There is an increase in delamination in the hole exit location due to increase in thrust force, which is evident.

The temperature of the composite increases in case of an increase in spindle speed [33], resulting in thermal softening, thereby reducing the torque and thrust force. Microscopic images are examined for machined holes at a constant speed and a point angle for different feeds, as shown in Figure 12. It is

Table 7. Experimental and predicted outputs for model verification.

no	Spindle speed (rpm)	Feed rate ($mm.rev^{-1}$)	Point angle (°)	Thrust force (F_z)			Torque (T)		
				Exp (N)	Pred (N)	Error (%)	Exp (Ncm)	Pred (Ncm)	Error (%)
1	750	0.125	85	83.04	82.43	0.73	30.45	29.71	2.43
2	750	0.075	118	58.64	57.92	1.23	24.19	24.51	−1.32
3	1250	0.075	118	54.11	55.70	−2.94	22.48	22.33	0.66
4	1250	0.125	135	90.57	87.23	3.69	35.65	34.56	3.06
				Delamination factor (F_d)			Diameter (D)		
				Exp	Pred	Error (%)	Exp (mm)	Pred (mm)	Error (%)
1	750	0.125	85	1.215	1.208	0.58	5.028	5.028	0.00
2	750	0.075	118	1.149	1.153	−0.35	5.031	5.029	0.04
3	1250	0.075	118	1.110	1.109	0.09	5.045	5.049	−0.08
4	1250	0.125	135	1.215	1.217	−0.16	5.032	5.033	0.02
				Cylindricity (ϕ)			Surface roughness (R_a)		
				Exp (mm)	Pred (mm)	Error (%)	Exp (μm)	Pred (μm)	Error (%)
1	750	0.125	85	0.011	0.0106	7.17	4.29	4.25	0.93
2	750	0.075	118	0.017	0.0165	5.24	3.69	3.67	0.54
3	1250	0.075	118	0.028	0.0267	3.44	4.28	4.33	−1.16
4	1250	0.125	135	0.023	0.0220	4.87	5.51	5.42	1.63

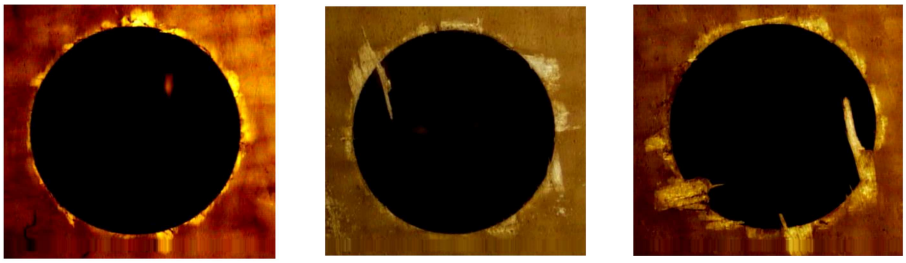

(a) (b) (c)

Figure 11. Images at exit location of drilled holes at constant spindle speed (1500 rpm) and feed (0.15 mm.rev^{-1}) for different point angles: (a) 85°, (b) 118°, and (c) 135°.

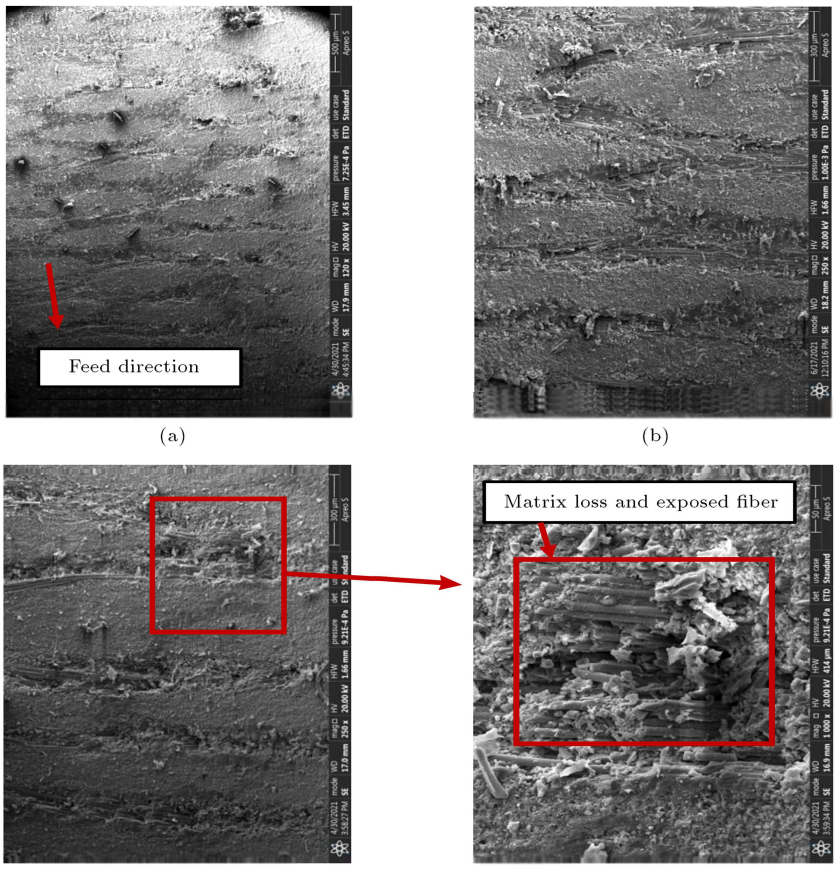

(a) (b)

(c) (d)

Figure 12. SEM images of machined holes at constant spindle speed (1500 rpm) and point angle (135°) for different feeds (mm.rev^{-1}): (a) 0.05, (b) 0.10, (c) 0.15, and (d) magnified image of the damage region.

observed that as the feed rate rises, the uncut chip thickness [34] increases, which increases the material to machine, thereby more rubbing as well as greater thrust force and torque. Due to increase in thrust force, irregularities and the damage in the hole wall tend to increase. The observed phenomenon of increase in thrust and torque due to higher feed [27,32,35] is shown in Figure 13(a) and (b).

As stated, the spindle speed increase leads to softening of matrix and reduction of the thrust force induced, eventually decreasing the hole delamination at the exit. Figure 13(c) also depicts the phenomenon that the high point angle and feed would increase the force induced in the process of drilling, due to which delamination at the exit of the drilled hole increases [14,27]. The observed phenomenon of experimental values for diameter and cylindricity of the hole is presented in Figure 13(d) and (e). Increase in the spindle speed attenuates the rotational stability of drill, which leads to more vibration and more increase in the diameter and cylindricity of the hole. Increase in feed rate results in lower cutting temperature and self-

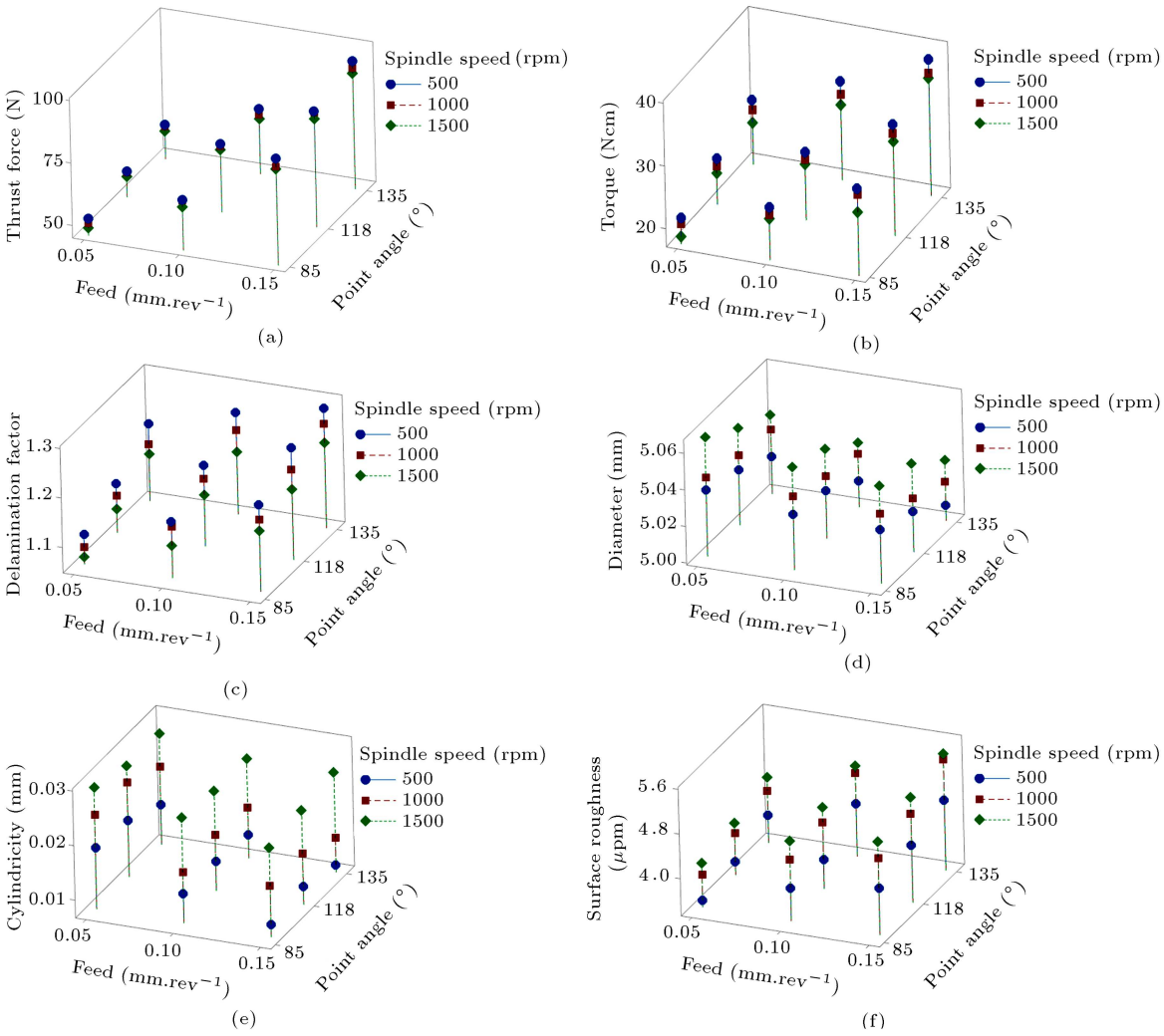

Figure 13. Scatter plots for the experimental values of output characteristics for (a) Thrust force (N), (b) torque (Ncm), (c) delamination factor, (d) diameter (mm), (e) cylindricity (mm), and (f) surface roughness (μm).

induced vibration, leading the diameter to be closer to the nominal one and yielding better cylindricity [35,36]. Surface roughness values obtained increase with increasing cutting speed and feed rate and the observed phenomenon is shown in Figure 13(f). It is emphasized that the prudent choice of the drilling input variables results in minimum damage induced due to drilling, leading to the improvement of composite part performance. Predictive model using ANN tool was developed to predict the output responses of drilled holes for the selected input variables in quartz polymeric composite laminate. The findings show good agreement and are in line with the experimental investigations. The reported results will help understand this material behavior when drilling operation is performed.

5. Conclusions

The present investigation aimed to develop a predictive model for estimation of torque, thrust force, and delamination factor at the hole exit, hole diameter, cylindricity, and surface roughness in the drilling of Quartz Cyanate Ester polymeric composite laminate specimen. To this end, experiments were performed as per FFD and BPNN model was developed using experimental data to compare the accuracy of predicted one with the experimental results. The developed model was further applied to a set of new experiments and the predicted model was validated. The following findings were drawn from the present research investigation.

- BPNN was employed to predict the output responses. Different BPNN architectures were developed and studied. Among those, 3-45-15-10-6 configuration (first, second, and third hidden layers with 45, 15, and 10 neurons as well as 3 and 6 neurons in the input and output layers) was attained as the best configuration for the present case and the mean square error of this developed architecture was 0.0105;

- BPNN successfully predicted torque, thrust force, delamination factor at exit, hole diameter, cylindricity, and surface roughness. The results of the developed neural network model were consistent with the directly measured values;
- Using developed BPNN model, maximum error was found to be 7.58% for the present case;
- New set of experimental studies was conducted for validation. Maximum error using the developed network model was found to be 7.17% for this case;
- Influence of input process variables on the output responses was studied. ANN- BPNN method was effective and acceptable since the maximum error between prediction and experiments was less than 10% in drilling of quartz polymeric composite.

Acknowledgment

The authors acknowledge Director, Advanced Systems Laboratory, DRDO, Hyderabad, India for providing continuous support and research facilities to carry out this work.

Nomenclature

GSM	Grams per Square Meter
V_f	Fiber volume fraction
DSC	Digital Scanning Calorimetry
NDE	Non-Destructive Evaluation
VARTM	Vacuum Assisted Resin Transfer Molding
N	Spindle speed
f	Feed
θ	Point angle
FFD	Full Factorial Design
WC	Tungsten carbide
F_d	Delamination factor
$D_{\max}$	Maximum diameter
D_0	Nominal diameter
R_a	Mean surface roughness
F_z	Thrust force
T	Torque
D	Hole diameter
ϕ	Cylindricity
η	Learning rate
β	Moving average parameter
MSE	Mean Squared Error
BPNN	Back Propagation Neural Network
ANN	Artificial Neural network

References

1. Donald, V.R. and Dominick, V.R., *Reinforced Plastics Handbook*, 3rd Edn., Elsevier (2005).
2. Nafiz, Y. and Mustafa, G. "The influences of varying feed rate on hole quality and force in drilling CFRP composite", *J of Science*, **30**, pp. 39–50 (2017).
3. Sorrentino, L., Turchetta, S., and Bellini, C. "A new method to reduce delaminations during drilling of FRP laminates by feed rate control", *Compos. Struct.*, **186**, pp. 154–164 (2018).
4. Won, M.S. and Dharan, C.K.H. "Drilling of aramid and carbon fiber polymer composites", *J of Manuf. Sci. and Eng.*, **124**, pp. 778–783 (2002).
5. Halil, B.K., Ali, U., Murat, K., et al. "A novelty optimization approach for drilling of CFRP nanocomposite laminates", *Int. J Adv. Manuf. Technol.*, **100**(9-12), pp. 2995–3012 (2019).
6. Chander, P., Alokesh, P., Animesh, K.B., et al. "Investigating the efficacy of adhesive tape for drilling carbon fibre reinforced polymers", *Materials*, **14**, pp. 1699–1716 (2021).
7. John, K.M. and Kumaran, S.T. "Backup support technique towards damage-free drilling of composite materials: A review", *Int. J Lightweight Mater. Manuf.*, **3**, pp. 357–364 (2020).
8. Davim, J.P. and Reis, P. "Study of delamination in drilling carbon fiber reinforced plastics (CFRP) using design experiments", *Compos. Struct.*, **59**(4), pp. 481–487 (2003).
9. Kishan, Z., Din, B., Soni, K., et al. "Recent trends in drilling of carbon fiber reinforced polymers (CFRPs): A state-of the art review", *J Manuf. Process.*, **69**, pp. 47–68 (2021).
10. Tsao, C.C. and Hocheng, H. "Taguchi analysis of delamination associated with various drill bits in drilling of composite material", *Int. J of Mach. Tools and Manuf.*, **44**(10), pp. 1085–1090 (2004).
11. Vijayan, K., Prabukarthi, A., Arun, R., et al. "Optimization of machining parameters at high speed drilling of carbon fiber reinforced plastic (CFRP) laminates", *Compos. B. Eng.*, **43**, pp. 1791–1799 (2012).
12. Anarghya, A., Harshith, D.N., Nitish, R., et al. "Thrust and torque force analysis in the drilling of aramid fibre-reinforced composite laminates using RSM and MLPNN-GA", *Heliyon*, **4**, p. 39 (2018).
13. Lee, J.H., Ge, J.C., and Song, J.H. "Study on burr formation and tool wear in drilling CFRP and its hybrid composites", *Appl. Sci.*, **11**(1), p. 384 (2021).
14. Kalita, K., Mallick, P.K., Bhoi, A.K., et al. "Optimizing drilling induced delamination in GFRP composites using genetic algorithm & particle swarm optimization", *Adv. Compos. Lett.*, **27**, pp. 1–9 (2018).

15. Ali, U., Murat, K., and Mehmet, B. "Optimization and effects of machining parameters on delamination in drilling of pure and Al_2O_3/SiO_2 added GFRP composites", Int. *J Adv. Manuf. Technol.*, **119**, pp. 657–675 (2022).

16. Ahmet, Y., Erol, K., Hisman, Y., et al. "Effects of cutting parameters and point angle on thrust force and delamination in drilling of CFRP", *Mater. Test.*, **56**, pp. 1046–1048 (2014).

17. Ramesh, B., Elayaperumal, A., Satishkumar, S., et al. "Effect of drill point geometry on quality characteristics and multiple performance optimization in drilling of nonlaminated composites", *Proc. Inst. Mech. Eng. L.*, **230**(2) pp. 558–568 (2016).

18. Karnik, S.R., Gaitonde, V.N., Rubio, J.C., et al. "Delamination analysis in high speed drilling of carbon fiber reinforced plastics (CFRP) using artificial neural network model", *Mater. Des.*, **29**(9), pp. 1768–1776 (2008).

19. Himmel, C., and May, P. "Advantages of plasma etch modeling using neural networks over statistical techniques", *IEEE Trans. Semicond. Manuf.*, **6**, pp. 103–111 (1993).

20. Yang, B., Fu, K., Lee, J., et al. "Artificial Neural Network (ANN) based residual strength prediction of Carbon Fibre Reinforced Composites (CFRC) after impact", *Appl. Compos. Mater.*, **28**, pp. 809–833 (2021).

21. Guoqiang, Z., Shabshan, H., and Hongqun, T. "Prediction of tool wear in CFRP drilling based on neural network with multicharacteristics and multisignal sources", *Adv. Compos. Lett.*, **30**, p. 15 (2021).

22. Qian, W. and Xiaoliang, J. "Multi-objective optimization of CFRP drilling parameters with a hybrid method integrating the ANN, NSGA-II and fuzzy C-means", *Compos. Struct.*, **235**, 111803 (2020).

23. Soepangkat, B., Norcahyo, R., Effendi, M.K., et al. "Multi-objective optimization in drilling kevlar fiber reinforced polymer using grey fuzzy analysis and backpropagation neural network - Genetic algorithm (BPNN-GA) approaches", *Int. J. Precis. Eng. Manuf.*, **20**, pp. 593–607 (2019).

24. Fajar, P.N., Soepangkat, B., Norcahyo, R., et al. "Multi response prediction of end milling CFRP with backpropagation neural network", *AIP Conf. Proc.*, **2114** (2019).

25. Vineela, M.G., Dave, A., and Chaganti, P.K. "Artificial neural network based prediction of tensile strength of hybrid composites", *Mater. Today*, **5**, pp. 19908–19915 (2018).

26. Mishra, R., Malik, J., Singh, I., et al. "Neural network approach for estimating the residual tensile strength after drilling in uni-directional glass fiber reinforced plastic laminates", *Mater. Des.*, **31**, pp. 2790–2795 (2010).

27. Soepangkat, B., Norcahyo, R., Effendi, M.K., et al. "Multi-response optimization of carbon fiber reinforced polymer (CFRP) drilling using back propagation neural network-particle swarm optimization (BPNN-PSO)", *Eng. Sci. and Technol.*, **23**, pp. 700–713 (2020).

28. Gaitonde, V.N., Karnik, S.R., and Davim, J. "Taguchi multiple-performance characteristics optimization in drilling of medium density fibreboard (MDF) to minimize delamination using utility concept", *J of Mater. Process. Techno.*, **196**, pp. 73–78 (2008).

29. Kuo, R. and Cohen, P. "Intelligent tool wear estimation system through artificial neural networks and fuzzy modelling", *Artif. Intell. Eng.*, **12**, pp. 229–242 (1998).

30. Mondal, N., Mandal, S., and Mandal, M.C. "FPA based optimization of drilling burr using regression analysis and ANN model", *Measurement*, **152**, 107327 (2020).

31. Zhang, C., Minda, Y., Chen, W., et al., *Gradient Descent Optimization in Deep Learning Model Training Based on Multistage and Method Combination Strategy*, Hindawi (2021).

32. Abhishek, K., Datta, S., and Mahapatra, S.S. "Optimization of thrust, torque, entry and exist delamination factor during drilling of CFRP composites", *Inter. J of Advan. Manuf. Techno.*, **76**, pp. 401–416 (2014).

33. Velayudham, A., Krishnamurthy, R., and Soundarapandian, T. "Evaluation of drilling characteristics of high volume fraction fiber glass reinforced polymeric composite", *Inter. J of Mach. Tools and Manuf.*, **45**, pp. 399–406 (2005).

34. Arshinov, V. and Alekseev, G., *Metal Cutting Theory and Cutting Tool Design*, MIR publishers, Moscow (1976).

35. Abhishek, K., Datta, S., and Mahapatra, S.S. "Multi-objective optimization in drilling of CFRP (polyester) composites: Application of a fuzzy embedded harmony search (HS) algorithm", *Measurement*, **77**, pp. 222–239 (2016).

36. Yaşar, N., Korkmaz, M.E., and Gunay, M. "Investigation on hole quality of cutting conditions in drilling of FRP composite", *MATEC Web Conf.*, **112** (2017).

Appendix A

Experimental and predicted outputs for all the responses are given in Tables A.1 and A.2.

Appendix B

The bar charts of the exprimental and predicted values for all the six output parameters of the training data are given in Figure B.1. Also, the comparison of all the six output parameters for the testing data set between prediction and experimental data is given in Figure B.2.

Table A.1. Experimental values and predicted outputs for thrust force, torque and delamination factor.

S No.	Spindle speed (rpm)	Feed rate (mm rev^{-1})	Point angle (°)	Thrust force (F_z)			Torque (T)			Delamination Factor (F_d)			Data type
				Experiment (N)	Predicted (N)	Error (%)	Experiment (Ncm)	Predicted (Ncm)	Error (%)	Experiment	Predicted	Error (%)	
1	500	0.10	85	65.07	65.713	–0.99	25.45	25.5407	–0.36	1.161	1.164	–0.39	Training
2	500	0.15	85	87.6	86.638	1.09	30.97	30.8687	0.33	1.223	1.219	0.05	Training
3	500	0.05	118	55.18	56.158	–1.77	24.32	24.1329	0.77	1.147	1.147	–0.69	Training
4	500	0.10	118	72.22	70.425	2.48	27.86	28.5942	–2.64	1.212	1.209	0.002	Training
5	500	0.15	118	91.31	92.103	–0.87	34.8	34.6113	0.54	1.274	1.264	0.46	Training
6	500	0.05	135	58.55	57.645	1.55	27.34	27.5731	–0.85	1.204	1.191	0.68	Training
7	500	0.10	135	70.92	70.932	–0.02	32.81	31.9084	2.75	1.254	1.250	–0.02	Training
8	1000	0.10	85	64.85	64.287	0.87	24.23	24.3109	–0.33	1.151	1.140	0.82	Training
9	1000	0.15	85	84.41	84.971	–0.67	29.97	29.4572	1.71	1.193	1.194	–0.35	Training
10	1000	0.05	118	54.66	54.599	0.11	23.16	22.9294	0.99	1.123	1.115	0.38	Training
11	1000	0.15	118	90.97	91.082	–0.12	33.43	33.6089	–0.54	1.230	1.225	0.34	Training
12	1000	0.10	135	68.53	70.604	–3.03	30.8	30.6855	0.37	1.219	1.210	–0.006	Training
13	1000	0.15	135	93.26	91.428	1.96	36.56	37.0449	–1.33	1.259	1.257	–0.59	Training
14	1500	0.05	85	47.84	47.273	1.18	18.31	18.5568	–1.35	1.062	1.057	0.23	Training
15	1500	0.10	85	62.22	62.756	–0.86	23.63	23.0522	2.44	1.113	1.117	–0.63	Training
16	1500	0.15	85	83.39	82.597	0.95	27.21	27.8091	–2.20	1.171	1.162	0.63	Training
17	1500	0.05	118	53.08	53.251	–0.32	22.06	21.3935	3.02	1.096	1.097	–0.69	Training
18	1500	0.10	118	69.9	68.746	1.65	25.94	26.1680	–0.88	1.152	1.149	0.044	Training
19	1500	0.15	118	88.24	89.393	–1.31	32.14	31.9572	0.57	1.191	1.189	0.04	Training
20	1500	0.05	135	56.1	55.893	0.37	23.72	24.2794	–2.36	1.142	1.134	0.51	Training
21	1500	0.15	135	91.12	90.516	0.66	35.87	35.16365	1.97	1.220	1.217	0.19	Training
22	500	0.15	135	96.18	91.862	4.49	38.86	38.0680	2.04	1.291	1.301	–0.88	Validation
23	1000	0.10	118	71.22	69.596	2.28	26.75	27.5419	–2.96	1.184	1.175	0.39	Validation
24	1000	0.05	135	57.91	56.711	2.07	25.72	26.1341	–1.61	1.163	1.155	0.36	Validation
25	500	0.05	85	51.51	51.239	0.53	21.3	20.7846	2.42	1.108	1.100	0.68	Testing
26	1000	0.05	85	49.65	49.037	1.23	20.4	19.6765	3.55	1.083	1.075	0.72	Testing
27	1500	0.10	135	67.02	70.390	–5.03	29.1	29.0052	0.33	1.175	1.180	–0.43	Testing

Table A.2. Experimental values and predicted outputs for diameter, cylindricity and surface roughness.

S No	Spindle speed (rpm)	Feed rate (mm rev^{-1})	Point angle (°)	Diameter (D)			Cylindricity (ϕ)			Surface roughness (R_a)			Data type
				Experiment (mm)	Predicted (mm)	Error (%)	Experiment (mm)	Predicted (mm)	Error (%)	Experiment μm	Predicted μm	Error (%)	
1	500	0.10	85	5.029	5.0304	–0.03	0.012	0.01218	–1.54	3.92	3.8681	1.32	Training
2	500	0.15	85	5.028	5.0272	0.015	0.009	0.00959	–6.56	4.16	4.2171	–1.37	Training
3	500	0.05	118	5.029	5.0287	0.005	0.017	0.01643	3.30	3.56	3.5157	1.24	Training
4	500	0.10	118	5.025	5.0238	0.023	0.012	0.01184	1.31	3.85	3.9177	–1.76	Training
5	500	0.15	118	5.021	5.0202	0.016	0.01	0.00952	4.80	4.36	4.3577	0 .05	Training
6	500	0.05	135	5.019	5.0195	–0.01	0.014	0.01482	–5.87	3.82	3.8463	–0.69	Training
7	500	0.10	135	5.013	5.0145	–0.03	0.011	0.01051	4.37	4.27	4.2480	0.51	Training
8	1000	0.10	85	5.039	5.0400	–0.02	0.016	0.01650	–3.13	4.43	4.4294	0.01	Training
9	1000	0.15	85	5.037	5.0361	0.02	0.016	0.01503	6.03	4.7	4.7038	–0 .08	Training
10	1000	0.05	118	5.037	5.0385	–0.03	0.024	0.02276	5.17	4.08	4.073 3	0.16	Training
11	1000	0.15	118	5.028	5.0296	–0.03	0.016	0.01584	0.98	4.92	4.917 1	0.05	Training
12	1000	0.10	135	5.028	5.0242	0.08	0.016	0.01697	–6.12	4.83	4.822 6	0.15	Training
13	1000	0.15	135	5.02	5.0205	–0.01	0.013	0.01397	–7.46	5.32	5.267 2	0.99	Training
14	1500	0.05	85	5.064	5.0618	0.04	0.029	0.02892	0.27	4.12	4.1847	–1.57	Training
15	1500	0.10	85	5.055	5.0564	–0.03	0.026	0.02518	3.15	4.76	4.7094	1.06	Training
16	1500	0.15	85	5.052	5.0527	–0.02	0.023	0.02353	–2.34	4.99	4.993 6	–0.07	Training
17	1500	0.05	118	5.052	5.0525	–0.011	0.027	0.02842	–5.26	4.26	4.2 418	0.43	Training
18	1500	0.10	118	5.048	5.0480	–0.001	0.025	0.02548	–1.93	4.79	4.7 768	0.28	Training
19	1500	0.15	118	5.047	5.0448	0.04	0.024	0.02445	–1.89	5.21	5.181 5	0.55	Training
20	1500	0.05	135	5.042	5.0423	–0.01	0.027	0.02679	0.75	4.5	4.5003	–0.006	Training
21	1500	0.15	135	5.032	5.0350	–0.06	0.025	0.02345	6.16	5.42	5.476 7	–1.05	Training
22	500	0.15	135	5.007	5.0106	–0.07	0.008	0.00805	–0.62	4.58	4.725 5	–3.18	Validation
23	1000	0.10	118	5.033	5.0334	–0.01	0.017	0.01805	–6.19	4.52	4.5301	–0.22	Validation
24	1000	0.05	135	5.034	5.0291	0.09	0.021	0.02066	1.60	4.26	4.3718	–2.63	Validation
25	500	0.05	85	5.035	5.0354	–0.01	0.018	0.01685	6.39	3.45	3.4393	0.31	Testing
26	1000	0.05	85	5.042	5.0459	–0.08	0.024	0.02218	7.58	3.91	3.9690	–1.51	Testing
27	1500	0.10	135	5.034	5.0381	–0.08	0.025	0.02431	2.76	4.96	5.0162	–1.13	Testing

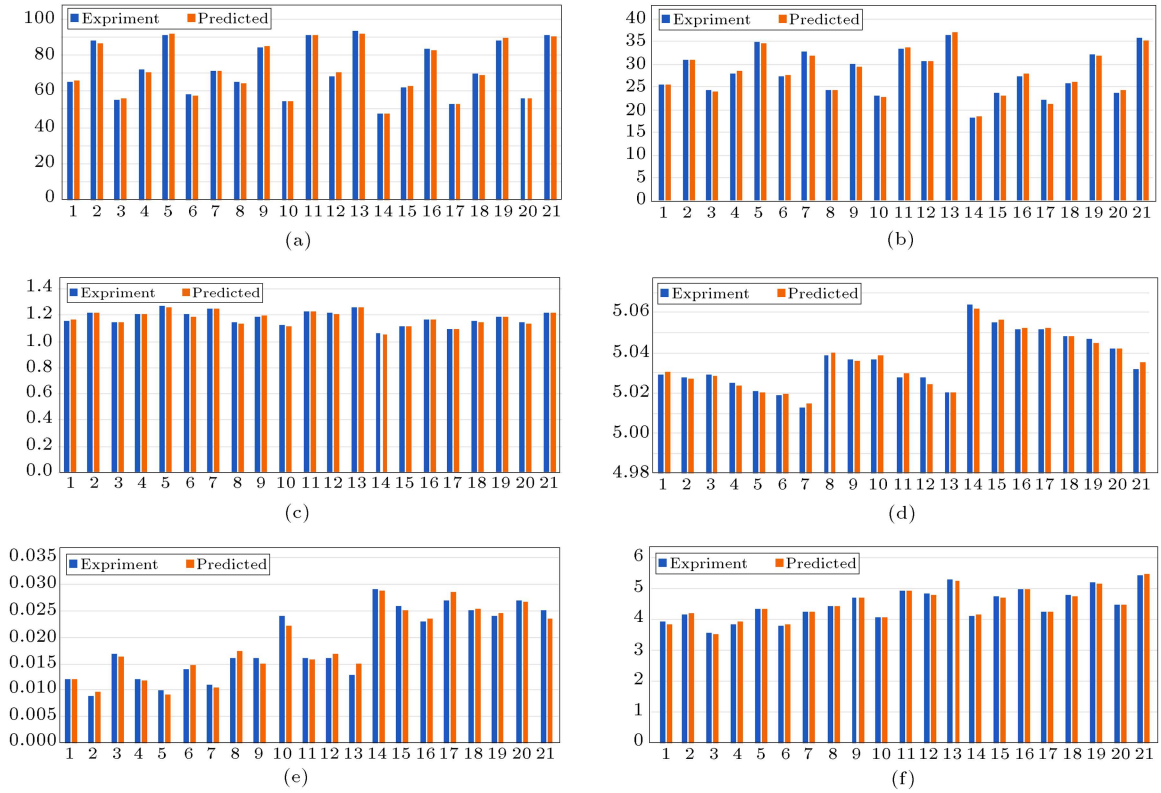

Figure B.1. Experimental and predicted output for training data for (a) Thrust force (N), (b) torque (Ncm), (c) delamination factor, (d) diameter (mm), (e) cylindricity (mm), and (f) surface roughness (μm).

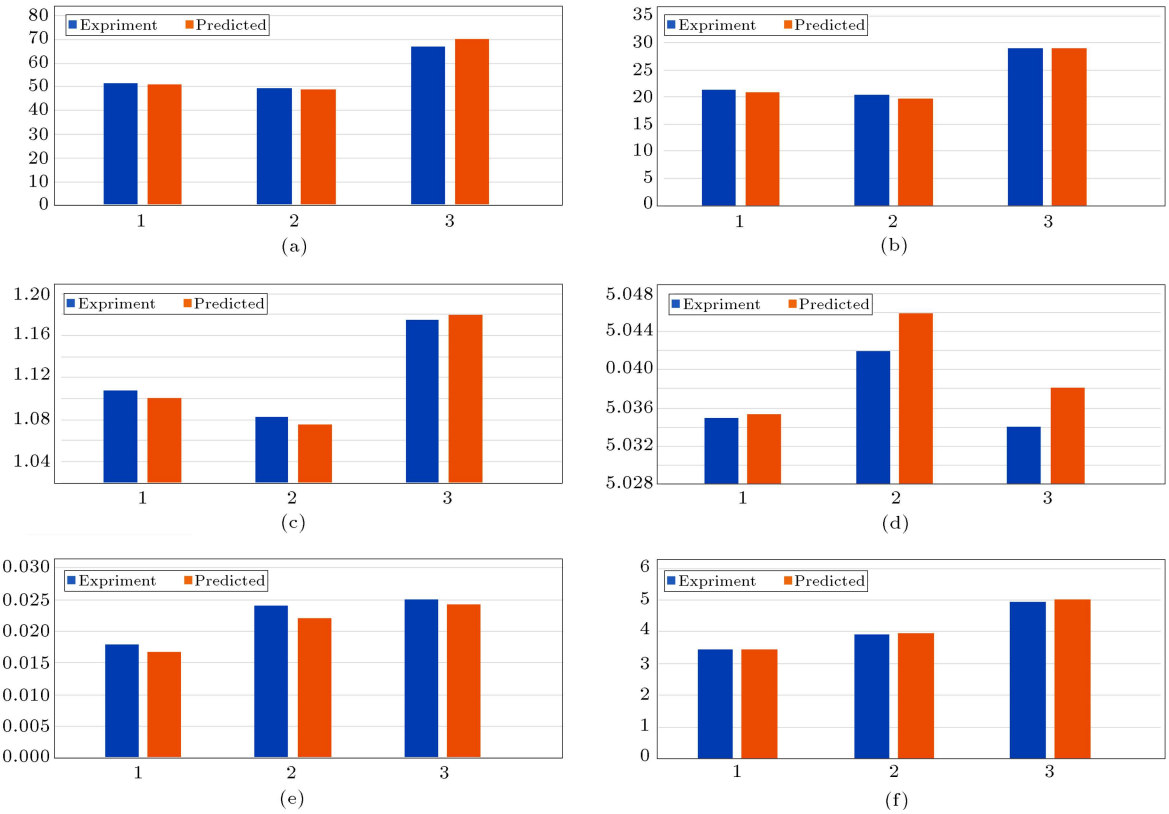

Figure B.2. Experimental and predicted output for testing data for (a) Thrust force (N), (b) torque (Ncm), (c) delamination factor, (d) diameter (mm), (e) cylindricity (mm), and (f) surface roughness (μm).

Biographies

Thiyagarajan Ramalingam, born in 1984, graduated in Mechanical Engineering from NIT Trichy, India in 2005. He is presently working as a Scientist 'F' in ASL, DRDO, Hyderabad, India and has about 16 years of experience in areas of polymeric composites materials, characterization, processes, machining methods, and technology/project management. His contribution in the current study includes conceptualisation, planning of experiments, specimen preparation, carrying out experiments, test results analysis, modeling, and conclusion.

Nayani Kishore Nath, born in 1972, obtained PhD from Osmania University, Hyderabad, India. He is presently working as a Scientist 'G' in ASL, DRDO, Hyderaba. He has been the recipient of various prestigious awards and has published more than 30 papers in various journals and conferences. He has given valuable suggestions on conducting the experiments and guidance for writing this paper.

Nagamuthu Selvaraj, born in 1963, obtained PhD from NIT Warangal, India. He is presently working as a Professor at MED, NIT Warangal. His research interests include modeling and simulation, flexible manufacturing system, CNC Technology, pull systems, machine tool, and composite materials. He has published more than 100 technical papers in international journals and international/national conference proceedings. In this study, he has given valuable suggestions on analyzing the test results and guidance for writing this manuscript.